A 1296-Cell Reconfigurable Reflect-Array Antenna With 2-Bit Phase Resolution for Ka-Band Applications

Enhao Wang, Guangyao Peng, Kunjing Zhong, Fan Wu, Zhi Hao Jiang, Ronan Sauleau, Wei Hong

A 1296-Cell Reconfigurable Reflect-Array Antenna With 2-Bit Phase Resolution for *Ka*-Band Applications

Enhao Wang, Guangyao Peng, Kunjing Zhong, Fan Wu, *Member*, *IEEE*, Zhi Hao Jiang, *Member*, *IEEE*, Ronan Sauleau, *Fellow*, *IEEE*, and Wei Hong, *Fellow*, *IEEE*

***Abstract*—A large-scale reconfigurable reflect-array antenna (RRA) with 2-bit phase resolution is reported here at *Ka*-band. The unit cell is designed based on a segmented resonator with end folding, which facilitates cell miniaturization and offers a stable angular response. By incorporating only two PIN diodes into each RRA unit cell, 2-bit phase compensation can be obtained due to the electronical reconfigurability of the resonant current path length. In order to validate the properties of the proposed 2-bit cells, a free-space scattering measurement of a uniform array is conducted. Furthermore, in order to construct large-scale extensible RRAs to meet versatile application demands, modular reflect-subarrays, each containing 144 RRA cells and their control module, are utilized as constitutive building blocks. As a demonstrative example, a 1296-cell RRA prototype fed by a broadband planar array is synthesized, fabricated, and characterized, yielding a peak gain of 29.2 dBi and an aperture efficiency of about 27.1% at 26.1 GHz. It experimentally achieves a beam scanning coverage up to ±50° with a 3-dB scanning loss. The demonstrated RRA is a promising candidate for future millimeter-wave communication and radar systems.**

***Index Terms*—2-bit phase compensation, beam-steering, millimeter wave, reconfigurable reflect-array (RRA).**

I. Introduction

Planar reflect-array antennas (RAs) contain the features of both the parabolic reflectors and phased array antennas by jointly utilizing the spatial illumination and phase synthesis technology [1]. Compared to the phased-array antennas relying on complex feed networks, the RAs do not suffer from insertion loss in the beam forming network, benefiting from the spatial feed scheme. The RA cells, which are the fundamental building blocks, function as reflective phase shifters, transforming the incident wave from the feed into collimated highly-directive beams or shaped beams [2]. A major shortcoming of the passive RAs is that they have a fixed beamforming functionality once the device is fabricated, thereby significantly restricting their widespread applications. In order to overcome this weakness, over the past decade, various reconfigurable techniques have been incorporated into the RA designs to achieve dynamically steerable beams [3], [4].

In general, the reconfigurable reflect-array antennas (RRAs) can be realized based on two different phase-shifting mechanisms. The first one provides a continuous reflection phase modulation, utilizing tunable materials [5], [6], rotatable micromotors [7], [8] or loaded varactor diodes [9], [10]. Basically, this method has the highest phase tuning accuracy, but requires a complex controlling system. Differently, the second type of RRAs is capable of enabling discrete phase shifting using electronic switches such as PIN diodes [11], [12] and microelectro-mechanical systems (MEMS) [13], [14], which possess lower reflection loss and simplified control circuits. Compared with PIN diodes, MEMS switches have lower DC power consumption and higher linearity, but this technology suffers from a high actuation voltage and low reliability. Therefore, due to the advantages with regard to loss, system complexity, and process maturity, RRAs based on PIN diodes have garnered a significant amount of attention in recent years.

The concept of 1-bit phase quantization features the lowest phase resolution, where a reflection phase difference of 180° can be obtained as the integrated devices are switched between the ON and OFF states. By incorporating lumped switches directly on the radiators [15], as well as loading diodes on the feeding probe of magneto-electric dipoles [16] or the phase delay line of patches [17-19], 1-bit RRAs supporting beams with single linearly/circularly polarization [15-20], polarization rotation, [21], [22] or multi-polarization [23-25] have been proposed, primarily at microwave frequencies within or below the *Ku*-band. A few demonstrations of 1-bit RRAs have also been carried out at millimeter-wave (mm-Wave) frequency bands by loading a PIN diode on the delay line of the patch in each cell [11], [26]. However, the 1-bit phase quantization introduces a quantization loss of about 3 – 4 dB, as compared to the RRAs with a continuous phase shifting [27], resulting in a low aperture efficiency and high sidelobe levels.

This work was supported in part by the National Natural Science Foundation of China (NSFC) under Grant 62122019, 62293492, and 61901106; in part by the ZTE Corporation and the State Key Laboratory of Mobile Network and Mobile Multimedia Technology. (*Corresponding author: Zhi Hao Jiang*)

Enhao Wang, Guangyao Peng, and Fan Wu are with the State Key Laboratory of Millimeter Waves, School of Information Science and Engineering, Southeast University, Nanjing 210096, China.

Zhi Hao Jiang and Wei Hong are with the State Key Laboratory of Millimeter Waves, School of Information Science and Engineering, Southeast University, Nanjing 210096, China, and also with Purple Mountain Laboratories, Nanjing 211111, China (e-mail: zhihao.jiang@seu.edu.cn).

Kunjing Zhong is with the State Key Laboratory of Mobile Network and Mobile Multimedia Technology, ZTE Corporation, Shanghai 201203, China.

Ronan Sauleau is with Univ Rennes, CNRS, Institut d'Electronique et des technologies du numérique (IETR) - UMR 6164, F-35000 Rennes, France.

In comparison, RRAs with 2-bit phase quantization possess improved performance in terms of the peak sidelobe level (SLL) and aperture efficiency, which are beneficial for far-field and near-field focusing, as well as imaging applications [28-30]. Several approaches have been proposed to achieve 2-bit phase-shifting. In [31], a 2-bit phase-shifting circuit with four loaded PIN diodes is attached to the radiator of an RRA cell. The realized LP cell-level possesses a bandwidth of 17.5% at *X*-band. The 90° phase difference between the cell states can also be achieved based on the effective geometrical rotation of the RRA cell [32], but only for circular polarization. A 2-bit CP RRA containing 16 × 16 cells, with each cell encompassing eight PIN diodes, is demonstrated at *X*-band, offering an aperture efficiency of 35% and a 3-dB beam scanning range of about ±60°. Furthermore, several other techniques have been applied for constructing dual-polarization 2-bit RRAs. In [33], a 2-bit cell containing four switches is devised for ±45°-linear polarizations by mixing two polarization-rotation modes and two non-polarization-rotation modes. Static array prototypes with 484 cells are experimentally characterized at *Ku*-band, showing a beam scanning up to 45° and an aperture efficiency of 39.4%. In [34], by the joint utilization of a current-reversal 180° phase shift and resonance shift induced 90° phase shift, a 2-bit 16 × 16-cell RRA is demonstrated at *S*-band, where each cell contains five PIN diodes, offering an aperture efficiency of 31.1% and a 3-dB beam scanning range of ±50°. In [35], a dual-LP 2-bit RRA cell with a bandwidth of 2.5% is proposed at *X*-band, consisting of two orthogonal crossed dipoles loaded with eight PIN diodes.

Due to their finer phase resolution, 2-bit RRAs require more delicately designed unit cells and more complex controlling circuitry, such that the majority of the demonstrated 2-bit RRAs work in the microwave bands below 11 GHz. At mm-Wave frequencies, these challenges become more severe, mostly due to the limited design space of the cells, stronger parasitic effects of PIN diodes, large-scale array realization, *etc*. Thus far, only a few attempts on mm-Wave 2-bit RRAs have been reported. In [36], based on a top polarization rotation layer and a bottom cross-shaped resonator providing a 90° transmissive and reflective phase shifting, respectively, a 2-bit RRA with 9 × 67 cells is proposed at *Ka*-band; in this case, each unit cell requires six MEMS switches. It supports a beam scanning range of ±30° and an aperture efficiency of 23.3%. Another 2-bit folded RRA design operating at 35 GHz is reported in [37], which is composed of 160 reconfigurable antenna-filter-antenna cells each containing five MEMS switches. It has an aperture efficiency of only 5.5% and a beam scanning range of ±45°. However, the fabricated arrays in these two works are "frozen" prototypes without the integration of realistic switches. Hence, it is highly desirable to achieve fully-functional 2-bit mm-Wave RRAs with steerable beams, which calls for higher demands on the integrability, reliability, and scalability of the RRA sub-system.

In this article, we report the design and experiment of a large-scale RRA with 2-bit phase resolution at *Ka*-band. A cell based on a segmented resonator with end folding and integrated with only two PIN diodes is proposed and validated, offering a stable 2-bit phase shift. In particular, the introduction of end folding effectively improves the angular response stability. The experimental results of a 2-bit RRA prototype with 36 × 36 cells highlight a wide beam scanning range and a high aperture efficiency. Compared to existing 2-bit RRAs in the mm-Wave bands, the proposed 2-bit RRA realizes fully-functional beam scanning with a superior performance. Furthermore, this work also provides a convenient and extensible system integration approach to the realization of large-scale RRAs for future mm-Wave communications.

This article is organized as follows. Section II presents the design, operation principle, and performance analysis of the proposed 2-bit RRA cell. Free-space measurement of the unit cell is reported in Section III. Section IV describes the synthesis, implementation, and characterization of the 36 × 36-cell RRA. Conclusions are drawn in Section V.

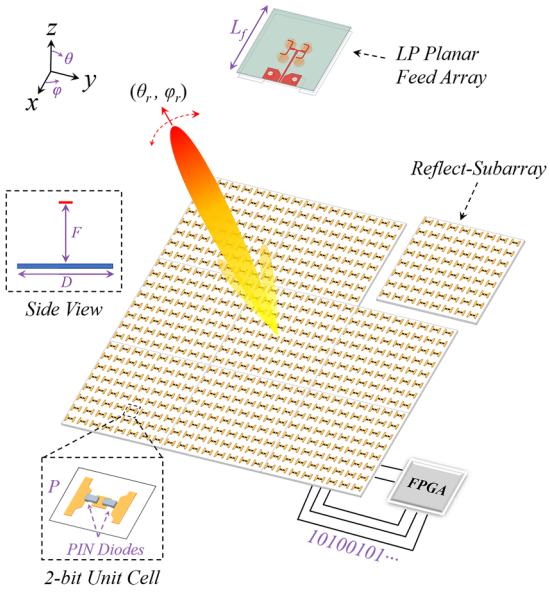

Fig. 1. 3-D schematic of the 2-bit LP RRA producing a steerable beam at (θ_r, φ_r) illuminated by a LP planar feed array. The reflect-array surface consists of 3 × 3 reflect-subarrays. The phase states are driven by a field-programmable gate array (FPGA) controller.

II. Design of 2-Bit mm-Wave RRA Unit Cells

The 3-D schematic of a 2-bit LP RRA containing 3 × 3 identical reflect-subarray modules is depicted in Fig. 1. Each RRA unit cell is capable of providing 2-bit phase compensation individually, where two PIN diodes are loaded to electronically adjust its working state. In order to minimize the feed blockage and reduce the overall profile of the RA antenna, a 2 × 2-element LP planar array is employed as the feed. The incident field is polarized along ***y***-direction. The *F*/*D* ratio is set to 0.87 so that the unit cells near the edges of the RRA are illuminated by waves with an incident angle of about 30°. The direct current (DC) biasing circuits are placed behind of the array, providing the desired biasing voltage to each PIN diode and, thereby allowing to steer electronically the antenna beam at (θ_r, φ_r).

A. RRA Unit Cell Design

The multi-layer structure of the proposed 2-bit RRA unit cell is illustrated in Fig. 2; it has a periodicity of 5 mm × 5 mm,

corresponding to $0.43\lambda_0 \times 0.43\lambda_0$ at the targeted center frequency around 26 GHz. It consists of three dielectric substrates and five metallic layers, in which the middle layer is a ground plane that isolates the mm-Wave resonator and biasing circuits [see Fig. 2(a)]. The segmented resonator with end folding for phase shifting is printed on the top dielectric substrate. It is composed of a central square patch and two unequal-sized parasitic patches [see Fig. 2(b)]. The outer ends of the two parasitic patches are folded downward and extended to the second metallic layer through two blind vias [see Fig. 2(c)]. This effectively gives rise to a miniaturized resonator by extending the resonant length and reduces capacitive inter-cell coupling. The central patch is electrically connected to the ground plane by using a metallic via for DC grounding. In the two gaps between the central patch and two parasitic patches, two PIN diodes, i.e. PIN 1 and PIN 2, are placed face-to-face for electrically adjusting the resonant state of the unit cell. Their anodes are directed to the parasitic patches, while the cathodes are connected to the central grounded patch. For welding the PIN diodes more precisely, two pads are added on the inner ends of the parasitic patches.

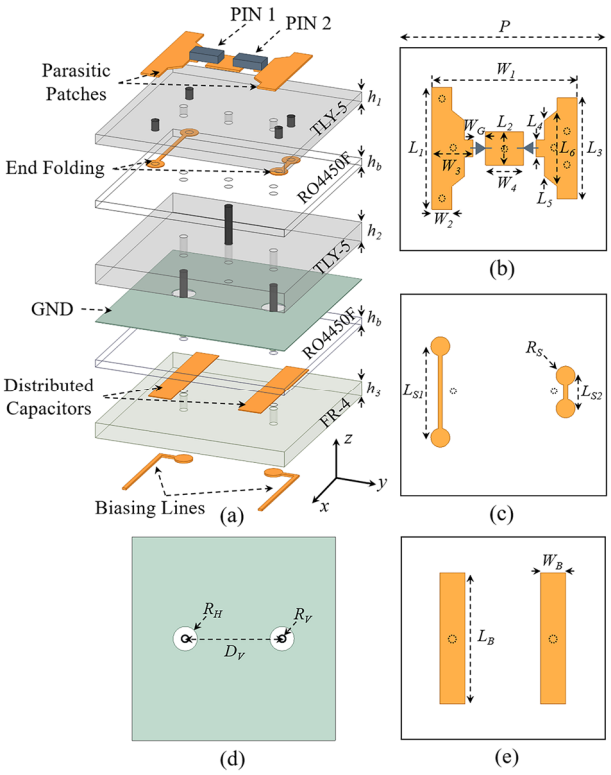

Fig. 2. Geometry of the proposed 2-bit RRA cell: (a) exploded view, (b) first layer, (c) second layer, (d) third layer, and (e) fourth layer. The optimized dimensions (all in millimeters) are $h_1 = 0.254$, $h_b = 0.2$, $h_2 = 0.508$, $h_3 = 0.4$, $P = 5$, $W_1 = 3.46$, $W_2 = 0.48$, $W_3 = 0.98$, $W_4 = 0.9$, $W_G = 0.3$, $W_B = 0.6$, $L_1 = 2.9$, $L_2 = 0.8$, $L_3 = 2.4$, $L_4 = 0.4$, $L_5 = 1.32$, $L_{S1} = 2.2$, $L_{S2} = 0.8$, $L_B = 3.1$, $R_S = 0.23$, $R_H = 0.6$, $R_V = 0.2$, and $D_V = 2.38$. The substrate materials are Taconic TLY-5 ($\varepsilon_r = 2.2$, $\tan\delta = 0.0009$) and FR-4 ($\varepsilon_r = 4.4$, $\tan\delta = 0.02$). The bonding film is Rogers 4450F ($\varepsilon_r = 3.52$, $\tan\delta = 0.004$).

In order to control independently the states of the two PIN diodes, biasing circuits need to be carefully designed. Two metallized via holes are used to connect the parasitic patches to the DC biasing lines on the bottom metallic layer, which go through two circular holes on the ground plane [see Fig. 2(d)]. Two rectangular pads are placed on the fourth metallic layer [see Fig. 2(e)], serving as distributed capacitors with an equivalent capacitance of about 0.78 pF [38]. Such a method is more effective than conventional RF choke circuits, such as radial stubs [26], [29], [32-36], and lumped inductors [34], [39], particularly at mm-Wave frequencies due to the limited available space and strong parasitic effects of the off-the-shelf lumped inductors. A full-wave simulation was conducted to show that the RF isolation is better than 27 dB in the operational band (not shown here for succinctness).

In order to drive electrically the RRA cells, commercially available off-the-shelf PIN diodes (MACOM MADP-000907-14020) are employed due to their low-loss properties at mm-Wave frequencies; the biasing voltage is 1.35 V for the ON state and 0 V for the OFF state, respectively. Importantly, since the reflection response of the RRA cells is sensitive to the parasitic effects of the diodes, which is more prominent at the mm-Waves, a precise knowledge of the equivalent circuit parameters of the PIN diodes is critical for an optimized RRA design. In order to accurately extract the equivalent circuit parameters, two methods have been followed as described in [40], including the through-reflect-line calibration of the PIN diodes and the measurement of the RRA unit cells in a WGS. We first characterized the PIN diode by using a microstrip through-reflect-line calibration setup, from which the initial values of the equivalent circuit parameters are extracted. Then, the circuit parameters of the PIN diode are experimentally validated and finely tuned by performing the cell measurement in a waveguide simulator iteratively [38] [see Fig. 3].

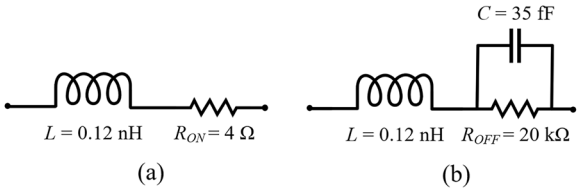

Fig. 3. Extracted equivalent circuit parameters of the PIN diode at (a) ON state and (b) OFF state.

TABLE I
OPERATION STATES OF THE 2-BIT RRA UNIT CELL

Phase State	PIN 1	PIN 2	Phase-shifting @ 26.1 GHz
00	OFF	OFF	270º
10	ON	OFF	180º
01	OFF	ON	90º
11	ON	ON	0º

The high-frequency structure simulator (HFSS) full-wave solver based on finite-element method is used to predict the scattering properties of the RRA cells; periodic boundaries and Floquet port excitation are employed [41]. In the numerical simulations, the lumped RLC boundaries are used to model the PIN diodes at the ON and OFF states. The four working states of the cell are referred to as "State 00", "State 10", "State 01", and "State 11", when the two PIN diodes are switched between "ON" and "OFF" states [see Table I]. The simulated reflection coefficients of the RRA cell at normal incidence are plotted in Fig. 4 for the four states. It can be seen that, at 26.1 GHz, the

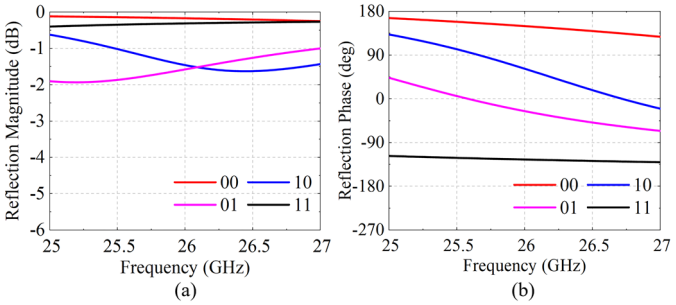

Fig. 4. Simulated reflection (a) magnitudes and (b) phases of the proposed RRA cell at normal incidence, for the 4 phase states.

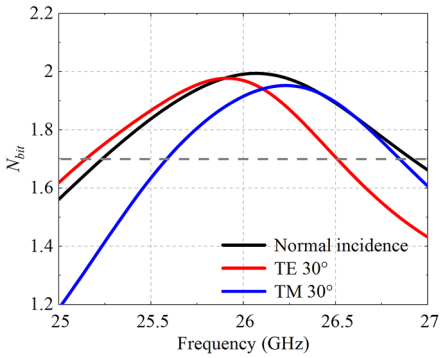

Fig. 5. Equivalent bit number N_{bit} of the proposed 2-bit RRA cell.

insertion loss of the cell is less than 1.5 dB, while the reflection phases are 147.9°, 53.2°, −30.5°, and −125.4° for States 00, 01, 10, and 11, respectively, achieving the desirable 2-bit phase quantization. In order to evaluate the performance of the RRA cell, two quantitative indicators are adopted, as [35]:

$$\sigma = \sqrt{\frac{\sum_{i=1}^{4}\left(\Delta\phi_i\right)^3}{12\times 360}}, \tag{1}$$

$$N_{bit} = \frac{\ln\left(\frac{360}{\sqrt{12}\sigma}\right)}{\ln 2}, \tag{2}$$

where $\Delta\phi_i$ is the phase difference between two adjacent cell states. For a 2-bit phase shifting cell (N_{bit} = 2), the ideal phase standard deviation σ is 26°. Its operational bandwidth can be defined as the frequency range within which σ is smaller than 32.5°, i.e., N_{bit} > 1.7. It can be seen from Fig. 5 that the bandwidth of 2-bit phase compensation covers from 25.2 to 26.9 GHz at normal incidence, with an averaged loss of less than 0.84 dB. The influence of the biasing lines on the reflection response of the RRA cells has been investigated as well. The results manifest that the scattering properties of the cells are hardly affected by the biasing lines, due to the good RF isolation and the fact that the orientations of the biasing lines and segmented end folding resonator are perpendicular to each other. Such a small impact of the biasing lines is beneficial to the realization of large-scale RRA prototypes.

B. Operating Principle of the RRA Unit Cell

In the design process of the proposed unit cell, first, the parasitic structures placed on the left and right sides (consisting of both the parasitic patch and its end folding) are constructed with the same geometrical. For such a symmetrical cell design, the reflection responses of State 10 and State 01 are the same, and they both have a phase difference of 135° with State 00 and State 11, as shown in Fig. 6(a). The desired phase difference between State 10 and State 01 can be further created by using different dimensions of the left and right parasitic structures. Specifically, by reducing the size of the right parasitic structure and increasing the size of the left parasitic structure, the resonant length of State 10 is shortened to produce a −45° phase shift, whereas the resonant length of State 01 is lengthened to obtain a 45° phase shift [see Fig. 6(b)]. As a result, a uniform phase difference of 90° between the four states can be achieved.

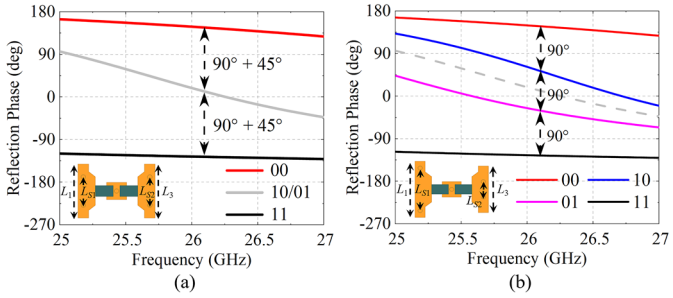

Fig. 6. Design evolution of acquiring the 2-bit reflection phase. (a) Simulated reflection phase of the symmetrical unit cell. The related dimensions are L_1 = 2.5, L_3 = 2.5, L_{S1}, = 0.65, and L_{S2} = 0.65. (b) Simulated reflection phase of the proposed. The related dimensions are L_1 = 2.9, L_3 = 2.4, L_{S1}, = 2.2, and L_{S2} = 0.8.

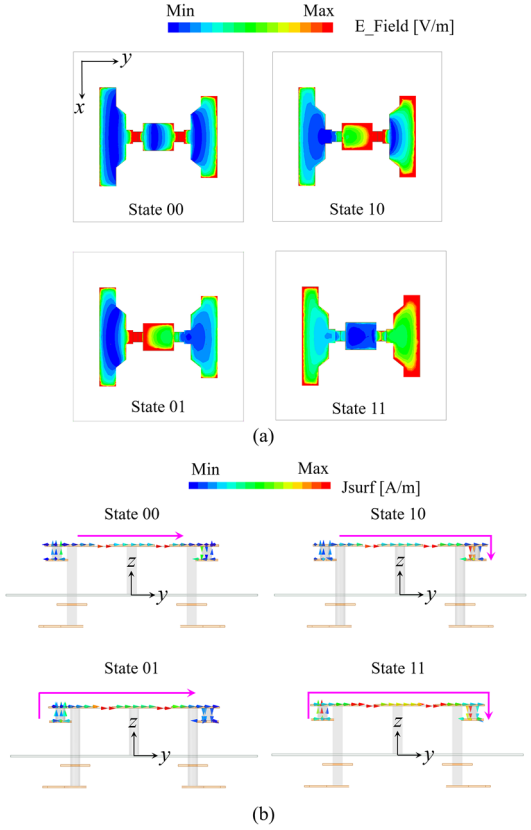

Fig. 7. Simulated (a) field distributions and (b) current distributions of the 2-bit unit cell.

In order to facilitate understanding of the working principle of the proposed RRA cell, the top views of field distributions

are given in Fig. 7(a) for the four different states; the current distributions on the segmented end folding resonator are also presented in Fig. 7(b). When both PIN diodes are "OFF", i.e., State 00, capacitive coupling between the central patch and parasitic patches is weak, yielding the shortest current path confined between the inner ends of the two parasitic patches. When PIN diode 1 or 2 is "ON" and the other is "OFF", the parasitic structure on the right or left side is excited, respectively. It should be noted that the currents will flow transversely (along the ***x***-direction) on both the parasitic patch and its end folding. Although the parasitic structure on the left is approximately the same length as the one on the right in the ***y***-direction, its length is longer in the ***x***-direction [see Fig. 7(a)]. Therefore, the current path lengths flowing on the resonator are different for these two cases. By changing the size of the two parasitic structures, the resonant frequency for State 01 happens at a lower frequency than that for State 10. This results in a phase difference of about 90° between these two states. Finally, at State 11, the two PIN diodes are both turned "ON", functioning as parasitic inductors. This allows for direct current flow between the central patch and parasitic patches, giving rise to a mode utilizing the entire folded resonator with the lowest resonant frequency among the four states. From this study, it can be concluded that switching the operating states of the PIN diodes modifies the resonant length of the RRA cell, thereby offering the desirable resonance shift induced 2-bit reflection phase compensation.

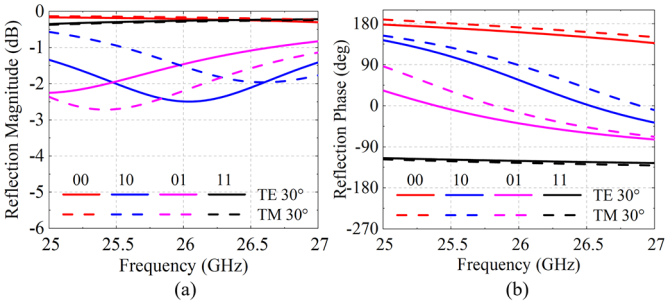

Fig. 8. Simulated reflection (a) magnitudes and (b) phases of the proposed 2-bit RRA cell at 30° oblique incidence for TE and TM polarizations.

C. Oblique Incidence Response of the RRA Unit Cell

The unit cells located in the outer region of the RRA are unavoidably illuminated under oblique incidence. For the proposed unit cell with its resonator aligned in the ***y***-direction, the planes of incidence for the transverse-electric (TE) and transverse-magnetic (TM) polarizations are the *x*-*z* plane and *y*-*z* plane, respectively. Here, an angle of incidence of θ_{inc} = 30° is considered, which is sufficient for RRA designs with a moderate focus-to-diameter (*F*/*D*) ratio of around 0.87. The simulated reflection magnitudes and phases of the unit cell under an oblique illumination of TE and TM polarized wave with θ_{inc} = 30° are presented in Fig. 8, respectively. It can be observed that the cell performance undergoes only a small variation as compared to that at the normal incidence. The averaged loss is lower than 1 dB at 26.1 GHz [see Fig 8(a)], which is 0.12 dB higher than that at normal incidence. The reflection phase differences are within 90±25° at 26.1 GHz under oblique illumination at θ_i = 30° for both TE and TM polarizations [see Fig. 8(b)]. Fig. 5 also presents the equivalent bit number N_{bit} of the proposed RRA cell under 30° incident angles. It can be seen that the cell exhibits an overlapped 2-bit phase compensation band spanning from 25.6 to 26.5 GHz for both polarizations with N_{bit} of greater than 1.94 at 26.1 GHz. Above all, these results manifest that a stable performance of the unit cell can be obtained at a 30° oblique incidence.

The cross-polarization levels under different incident angles are also studied. They are below −60 dB as θ_i varying from 0° to 30° for TM polarization in the operational band. However, the cross-polarization levels increase under the TE-polarization due to the presence of the vertical vias. It is still below −20 dB at θ_i = 30° for most cell states. Consequently, the cross-polarization of the final 1296-cell RRA will not be degraded.

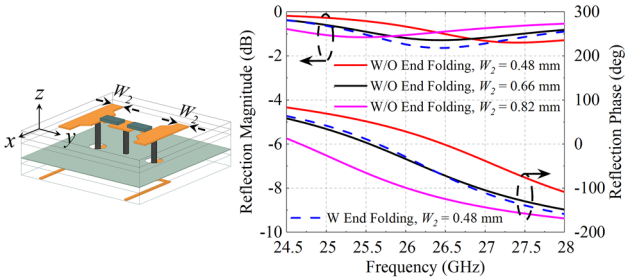

Fig. 9. (a) Configuration of the 2-bit RRA cell without end folding on the segmented resonator. (b) Simulated reflection coefficients with various widths of the parasitic patches (W_2) at State 10.

D. Comparison of Cell Designs With/Without End Folding

In order to understand the effect of the end folding structures on the cell design, a reference RRA cell without any folding is designed for comparison [see Fig. 9(a)]. The influence of varying the value of W_2, which controls the length of the resonator, on the reflection coefficients of the cell is reported in Fig. 9(b) for normal incidence. For succinctness, only the case of State 10 is presented. It can be readily found that the reference cell shares a similar resonant response as that of the proposed cell, when W_2 is equal to 0.66 mm. This indicates that the end folding leads to a reduction of the resonant length along the ***y***-direction for the segmented resonator of the RRA cell.

TABLE II
PHASE STANDARD DEVIATION AND BIT NUMBER OF THE REFLECTION PHASES BETWEEN THE PROPOSED AND REFERENCE RRA UNIT CELLS

θ_{inc} (°)	TE-Polarization				TM-Polarization			
	With End Folding		Without End Folding		With End Folding		Without End Folding	
	σ (°)	N_{bit}	σ (°)	N_{bit}	σ (°)	N_{bit}	σ (°)	N_{bit}
0	26.1	2.0	25.8	2.0	26.1	2.0	26.1	2.0
10	26.1	2.0	25.8	2.0	26.1	2.0	26.0	2.0
20	26.2	2.0	26.2	2.0	26.3	2.0	26.8	2.0
30	26.9	1.9	27.3	1.9	27.0	1.9	31.0	1.7
40	29.1	1.8	30.7	1.8	28.3	1.9	39.7	1.4

Importantly, the folded configuration facilitates a better angular stability of the cell properties. The comparisons of the phase standard deviation σ and bit number N_{bit} between the proposed and reference cells at 26.1 GHz under oblique

incidence are given in Table II. As the incident angle varies from 0° to 40°, the performance of both cells gradually deteriorates. The reflection phase variations of the two cells are stable when the cells are illuminated by a TE polarized wave, both exhibiting N_{bit} = 1.8 at 40° incident angle. However, for TM polarization, the two cell designs exhibit distinct behaviors at large incident angles. When the incident angle is increased to 40°, the reference cell suffers from a larger deviation with σ = 39.7°, corresponding to N_{bit} = 1.4, whereas the proposed cell exhibits a much better performance of σ = 28.3° and N_{bit} = 1.9. The more robust angular response of the proposed cell is primarily attributed to the reduced spatial dispersion and inter-cell coupling along the ***y***-direction.

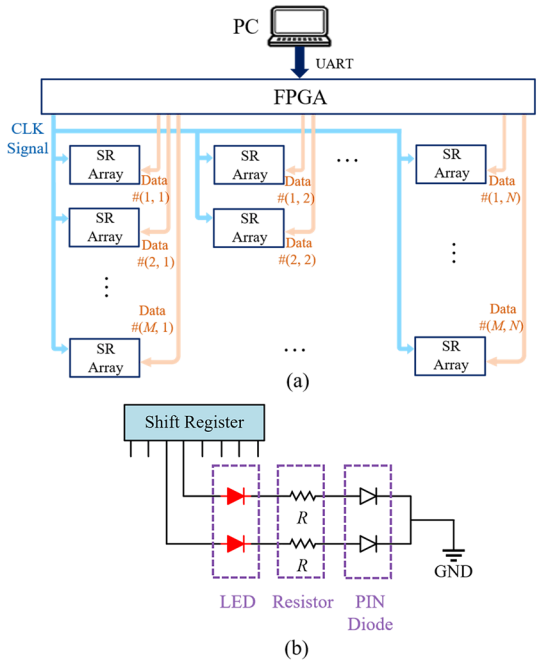

Fig. 10. Diagram of (a) the controlling module of the RRA with $M \times N$ reflect-subarrays, and (b) the electrical signal control of the PIN diodes in a unit cell.

III. Free-Space Characterization of RRA Unit Cells

In order to validate the proposed 2-bit RRA cells, a free-space scattering measurement [18], [19] is conducted. For evaluating the cell performance in a practical array environment, a 24 × 24-cell finite RRA with identical cell working states is fabricated and illuminated by a distant horn antenna.

A. RRA Fabrication

First, a 12×12-cell reflect-subarray is implemented and fabricated. Such kind of subarray can be used as constitutive building blocks to construct RRAs with different sizes of the radiating aperture for specific application requirements, offering a convenient and extensible approach.

To provide the cells each with a proper biasing voltage, a controlling module for an extensible RRA with a number of ($M \times N$) reflect-subarrays is designed. As shown in Fig. 10(a), the control module consists of a personal computer (PC), an FPGA controller, and $M \times N$ shift register (SR) arrays. Each subarray contains 36 SRs for sending high- and low-level DC voltage signals to the 288 PIN diodes. The FPGA delivers the clock (CLK) signals and data signals (through data channels 1 – MN) to each SR array such that each cell can be independently adjusted. In addition, a light emitting diode (LED) along with a voltage-dividing resistor is connected in series with each PIN diode to provide a working voltage of 1.35 V [see Fig. 10(b)]. This offers a visualization of the working states of all the PIN diodes, facilitating the array debugging as well.

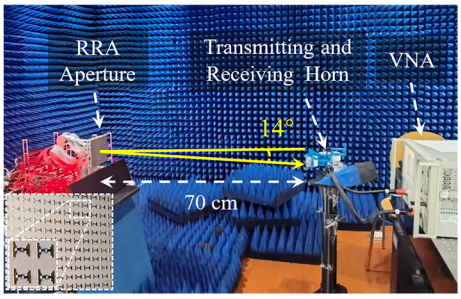

Fig. 11. Free-space scattering measurement of a 24 × 24-cell RRA.

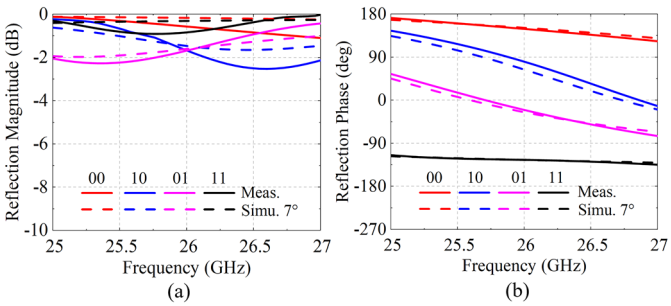

Fig. 12. Measured and simulated free-space reflection (a) magnitudes and (b) phases of the 576-cell RRA containing 2 × 2 reflect-subarrays.

B. Free-Space Scattering Measurement

In order to acquire more accurate measured results, an RRA composed of 2 × 2 reflect-subarrays is employed, with a size of 120 mm × 120 mm. A transmitting horn and a receiving horn are used to illuminate the RRA and collect the signal reflected from the RRA, which are connected to a vector network analyzer (VNA) [see Fig. 11]. The two horns are placed at a distance of 70 cm from the RRA aperture with a small separation in between, corresponding to an incident angle of about 7° with a TM polarization. During the experiments, all the 2-bit RRA cells are simultaneously adjusted to the same working states such that the aperture has a uniform reflection phase with a step of 90°, resulting in strong reflection in the specular direction. After using the time domain gating [43] in VNA and calibrating the results with a metallic plate of the same size, the measured reflection coefficients of the uniform RRA can be obtained. As shown in Fig. 12, at 26.1 GHz, the insertion loss is less than 1.9 dB, while the reflection phases are 148.5°, 50.7°, −32.9°, and −125.6° for State 00 – State 11, respectively. The equivalent bit number N_{bit} is greater than 1.7 with an averaged reflection loss of below 1.11 dB from 25.4 to 27 GHz. The slight deviations between the measured and simulated results are mainly due to fabrication and soldering inaccuracy, as well as the difference between the configurations considered in the measurement (scattering of a finite-sized RRA) and simulation (scattering of an infinite periodic array).

IV. Demonstration of a Large-Scale 2-Bit RRA Containing 36 × 36 Unit Cells at Ka-Band

Based on the validated cell design, a large-scale 2-bit RRA containing 36 × 36 unit cells, i.e., ~1300 cells is implemented, which is fed by a compact planar array. The radiation properties of the RRA prototype are characterized and analyzed.

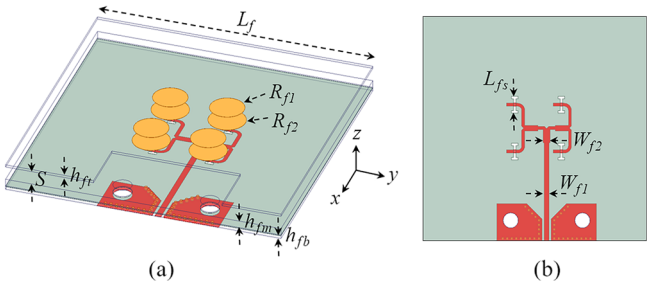

Fig. 13. (a) Configuration of the LP planar feed array. (b) Planar view of the feeding layer. The optimized dimensions are h_{f1} = 0.254, h_{fm} = 0.787, h_{fb} = 0.1, S = 1.5, R_{f1} = 1.85, R_{f2} = 2, L_f = 30, L_{fs} = 2.24, W_{f1} = 0.64, and W_{f2} = 0.91, all in millimeters. The substrate materials are Taconic TLY-5 (ε_r = 2.2, tanδ = 0.0009) and RO4003 (ε_r = 3.55, tanδ = 0.0027). The bonding film is Rogers 4450F (ε_r = 3.52, tanδ = 0.004).

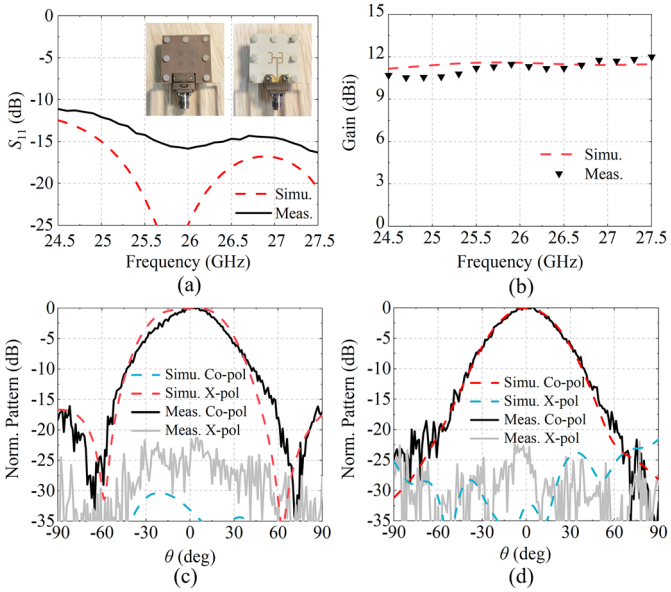

Fig. 14. Simulated and measured (a) S_{11}, (b) peak gain, and normalized radiation patterns at 26.1 GHz in the (c) y-z plane and (d) x-z plane of the planar feed array.

A. LP Planar Feed Array

Horn antennas have been commonly employed as the feed source for RRAs, which inevitably causes feed blockage and increases the overall profile [12]. Here, an LP planar array antenna composed of 2 × 2 aperture-coupled elements is adopted to serve as the feed, which provides a stable radiation performance over a broad band and a compact footprint of 30 mm × 30 mm [see Fig. 13(a)]. Each element contains a driven patch printed on the Taconic TLY-5 substrate with a thickness of 0.254 mm and a parasitic patch printed on the same substrate with a different thickness of 0.787 mm. An air spacer is added to provide proper inter-patch coupling. The feeding circuitry of the array, shown in Fig. 13(b), is printed on the Rogers RO4003 substrate with a thickness of 0.304 mm. The patches are excited by the microstrip feeding network through four slots cut on the metallic ground. A bonding film of Rogers 4450F with a thickness of 0.1 mm is used to combine the Taconic TLY-5 and the Rogers RO4003 substrates.

The planar feed array was fabricated, assembled, and characterized [see inset of Fig. 14(a)]. A southwest microwave connector was installed to perform the measurement. As shown in Fig. 14(a), the simulated S_{11} is less than −16 dB while the measured S_{11} is below −12 dB from 25.1 to 27.5 GHz, indicating a broad impedance matched band. The radiation patterns of the planar array were measured in a far-field anechoic chamber. The simulated and measured peak gains as a function of frequency are given in Fig. 14(b), showing a value of 11.6 dBi at 26.1 GHz. The fluctuation of the peak gains is less than 1.5 dBi from 25.1 to 27.5 GHz. At 26.1 GHz, a good agreement between the simulated and measured normalized radiation patterns is obtained in both the y-z and x-z planes [see Fig. 14(c) and (d)]. The measured results show a roll-off of 5.2 dB and 6.7 dB at an angle of ±30° off broadside in the y-z and x-z plane, respectively. The measured cross-polarization levels are below −21 dB in both two planes, implying a high polarization purity.

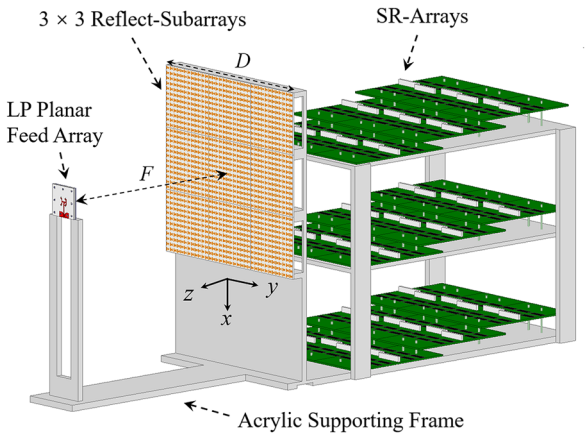

Fig. 15. Architecture of the RRA composed of 3 × 3 reflect-subarrays backed by the controlling modules.

B. Architecture, Synthesis, and Implementation of RRA

Once the feed source, unit cell, and the controlling modules have been designed and verified, the architecture of a large-scale RRA can be constructed [see Fig. 15]. It is composed of 3 × 3 reflect-subarrays each containing 12 × 12 cells, i.e. a total of 1296 cells. The planar feed array is located in front of the RRA to provide a spatial excitation. The F/D ratio is set to 0.87 with the edge taper of the RRA aperture of about −5.5 dB. The subarrays are tightly fixed to an acrylic supporting frame with a thickness of 5mm using a hot-melt adhesive, thereby ensuring a good flatness of the aperture. Each subarray is equipped with an SR-array connected through six flexible-flat-cables [see Fig. 16(a)]. To facilitate the connection of the biasing cables, the SR-arrays are mounted on three separate layers, which could be made more compact if needed. It should be noted that, by virtue of the modular subarray design, the employed layout can also be assembled and extended flexibly to form RRAs with a larger scale or other aperture shapes. In addition, approximately only

a half of the PIN diodes operates at the "ON" state for different beams. Accordingly, the total power consumption of the whole RRA is estimated to be about 17.5 W.

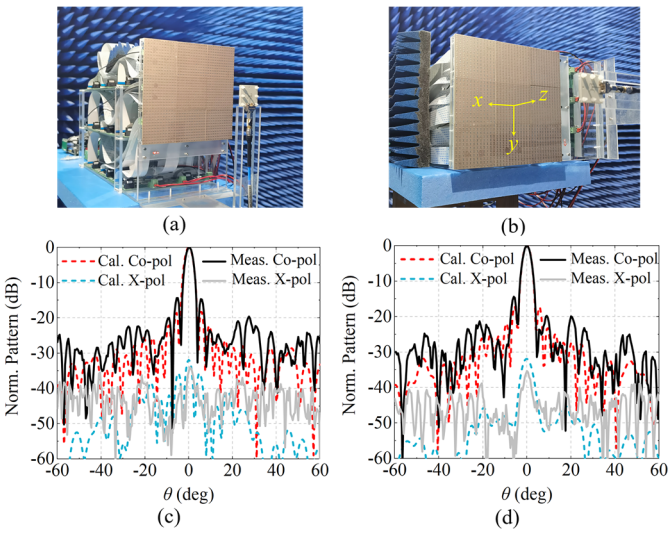

Fig. 16. Measurement setup for beam scanning in the (a) *y-z* plane and (b) *x-z* plane. Calculated and measured normalized radiation patterns of the broadside beams at 26.1 GHz in the (c) *y-z* plane and (d) *x-z* plane.

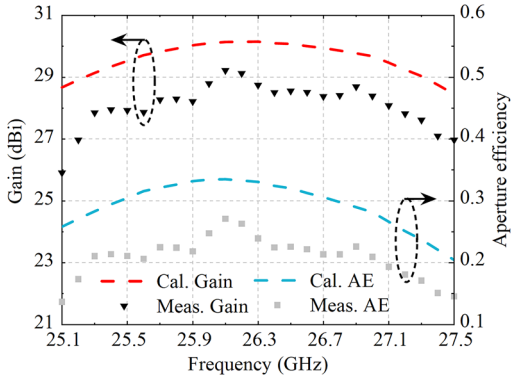

Fig. 17. Calculated and measured peak gain and aperture efficiency as a function of frequency for the broadside beam.

To evaluate the radiation performance of the RRA, a semi-analytical method based on the vectorial near-field quantities and scattering parameters of the unit cells for the efficient array synthesis is utilized [43]. The calculated 2-D normalized radiation patterns of the broadside beams in the *y-z* and *x-z* planes at 26.1 GHz are plotted in Fig. 16(c) and (d), respectively. A pencil beam pointing to $\theta = 0°$ is obtained in both of the orthogonal main planes, showing the 3-dB beamwidth of about 2.5° and an SLL of less than −17.7 dB. The calculated cross-polarization level is less than −32 dB in both planes. The calculated peak gain and aperture efficiency values of the broadside beam at different frequencies are shown in Fig. 17, showing a peak gain of 30.2 dBi and a maximum aperture efficiency of 33.5%. Furthermore, the radiation patterns of the beam scanning from −60° to 60° in both planes are also calculated. As shown in Fig. 19, the calculated radiation patterns exhibit a high accuracy of beam direction with an averaged scanning angle error of about 0.3°/0.2°/0.7° and a peak SLL of below −15/−15.5/−15.9 dB in both *y-z* and *x-z* planes at 25.7/26.1/27 GHz. The calculated beam scanning range is about ±45° in both planes for a 3-dB scan loss at these three frequency points.

To manifest the superiority of 2-bit phase resolution, we made a comparison between the 1-bit and 2-bit RRAs using the same cell design by observing the calculated broadside radiation pattern in the *y-z* and *x-z* planes [see Fig. 18(a) and (b)]. The 1-bit RRA uses two cell states with a 180°-phase difference. It can be seen that the calculated gain values of the broadside beam are 30.14 dBi and 27.37 dBi for the 2-bit and 1-bit RRAs, respectively, corresponding to aperture efficiency of 33.5% and 17.7%. Moreover, the SLLs of RRA with 2-bit phase quantization are less than −17.7 dB, whereas the peak SLL of the 1-bit RRA can be as high as −13.2 dB. This comparison clearly indicates that the 2-bit scheme is significantly superior to the 1-bit RRA in terms of both SLL and aperture efficiency. Although the biasing lines of the 2-bit RRAs are generally more complicated than that of the 1-bit RRAs, in our work, only two biasing lines are required to control the states of the PIN diodes. The number of switch components is also smaller than the other reported 2-bit RRAs listed in TABLE IV, so the increase of complexity is acceptable. In addition, it should be mentioned that in order to have a similar gain values, the area of the array needs to be doubled by using the 1-bit cells, which will lead to a much larger footprint, higher cost, and increased complexity.

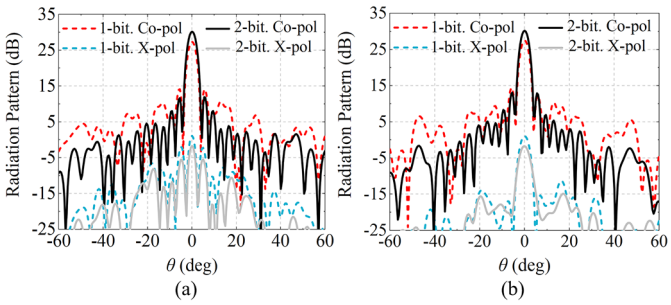

Fig. 18. Calculated radiation patterns between 1-bit and 2-bit phase resolution in the (a) *y-z* plane and (b) *x-z* plane.

C. *Measurement and Discussion*

For experimental verification, the 2-bit RRA prototype with 36 × 36 cells was measured in a far-field anechoic chamber. The 2-D beam scanning performance of the RRA was experimentally verified in the *y-z* and *x-z* planes. Because of the setup of the rotating table in the chamber, the entire RRA system needs to be rotated by 90° for the pattern measurements in the *x-z* plane [see Fig. 16(a) and (b)]. The measured normalized radiation patterns of the broadside beams in the *y-z* and *x-z* planes at 26.1 GHz are shown in Fig. 16(c) and (d), respectively. It can be readily seen that the pencil beam points to $\theta = 0°$ in the two orthogonal main planes, showing a good agreement between the calculated and measured results. The measured 3-dB beamwidth is 2.7°, while the measured SLL is smaller than −14.4 dB in both planes, respectively. The slightly higher SLL is primarily due to the phase compensation error. It was tested that approximately 90 cells were found faulty due to the fabrication inaccuracy of the RRA printed circuit boards and failed diode welding. Besides, slight warpage of the fabricated

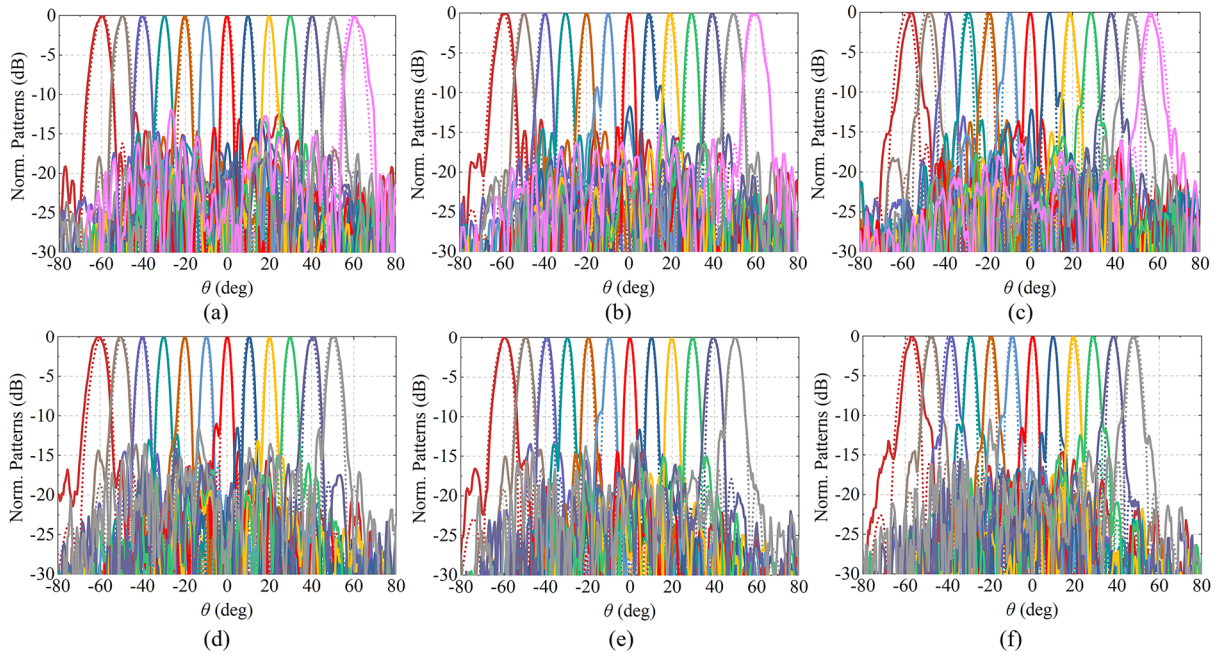

Fig. 19. Calculated (dashed lines) and measured (solid lines) normalized radiation patterns of the 2-bit RRA in the *y*-*z* plane at (a) 25.7 GHz, (b) 26.1 GHz, and (c) 27 GHz, and *x*-*z* plane at (d) 25.7 GHz, (e) 26.1 GHz, and (f) 27 GHz.

reflect-subarrays leads to a surface misalignment of about 1 mm across the aperture. These multiple factors would lead to phase compensation error and thus a relatively higher measured SLL. The measured cross-polarization level is below −34 dB, indicating that the beam generated by the RRA possesses a high cross-polarization purity. The peak gain and aperture efficiency of the broadside beam at different frequencies are also examined from 25.1 to 27.5 GHz [see Fig. 17], showing maximum values of 29.2 dBi and 27.1% at 26.1 GHz, respectively. The difference between the calculated and measured peak gains is on average value of 1.47 dB from 25.2 to 26.9 GHz. The variation of peak gain is within 1 dB in the band of interest from 25.7 to 27.0 GHz.

TABLE III
LOSS BUDGET FOR THE BROADSIDE BEAM AT 26.1 GHZ

Loss Factor	Values (dB)	Percentage (%)
Ideal Directivity	34.88	100
Cell Reflection Loss	0.9	81.3
Phase Quantization Loss	0.9	81.3
Feed Loss	0.63	86.5
Spillover Loss	2.35	58.2
Illumination Loss	0.63	86.5
Others	0.25	94.4
Measured Gain	29.22	27.1

The loss budget of the RRA prototype is listed in Table III, where the quantities are derived from simulations. The averaged cell reflection loss is about 0.9 dB as presented in Section II. Compared to the ideal phase compensation, the loss due to the 2-bit phase quantization is 0.9 dB. The simulated radiation efficiency of the feed array is 86.5%, which leads to a feed loss of 0.63 dB. In addition, the spillover loss and illumination loss are 2.35 dB and 0.63 dB, respectively. Although the planar feed arrays have advantages in terms of the overall profile and the system integration, they indeed would cause issues such as a relatively higher absorption loss and/or a larger spillover loss. It is believed that these could be improved by designing a more efficient low-profile feed antenna with a shaped beam in future work. The rest of the loss is about 0.25 dB, mainly coming from the faulty cells and imperfect assembly. From the analysis of the loss budget, it can be seen that the loss mainly comes from the feed spillover.

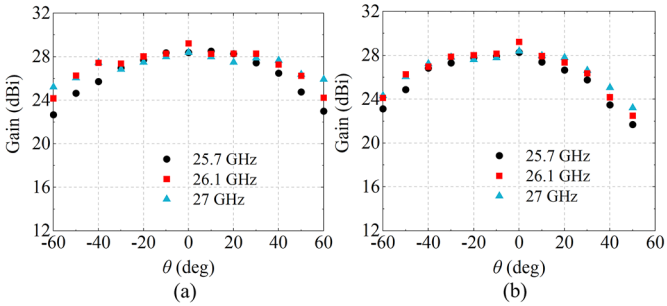

Fig. 20. Measured gains with different scanning angles in the (a) *y*-*z* plane and (b) *x*-*z* plane.

When the controlling module delivers different coding sequences to the RRA, a steerable high-gain beam can be generated. The normalized measured radiation patterns of the scanned beam at three operating frequency points are shown in Fig. 19. In both planes, the measured beam patterns match well with the calculated results. It can be seen that the measured SLLs are below −15 dB for most of the beams, while a few beams have a slightly higher SLL due to the faulty cells and phase compensation errors. In the *y*-*z* plane, the 3-dB beamwidth broads from 2.7° to about 4.7° as the beam steers away from broadside to 60° off normal. The beam scanning range with a 3-dB scan loss is ±50° at 26.1 GHz, while the scan

TABLE IV
COMPARISON AMONG DIFFERENT RRAS WITH DISCRETE PHASE-RESOLUTION

	[26]	[11]	[35]	[31]	[34]	[32]	[36]*	[37]*	This work
Freq. (GHz)	28	60.25	8	10	2.3	9.5	30	35	26.1
Phase Resolution	1-bit	1-bit	2-bit	2-bit	2-bit	2-bit	2-bit	2-bit	2-bit
Component Type, Number per Pol.	PIN diode, 1	PIN diode, 1	PIN diode, 4	PIN diode, 4	PIN diode, 2.5	PIN diode, 8	MEMS, 3	MEMS, 2.5	PIN diode, 2
Array Scale	400 Cells	25600 Cells	Cell Level	Cell Level	256 Cells	256 Cells	160 Cells	160 Cells	1296 Cells
Type of Feed	Horn	Horn	/	/	Horn	Horn	Leaky Wave	Horn	Planar Array
Peak Gain (dBi)	21.3	42	/	/	21.7	24.5	27.8 (passive)	15.3 (passive)	29.2
2-dB Gain Bandwidth (%)	N.A	N.A	/	/	>15.2	21.5	N.A	N.A	8
Aperture Efficiency (%)	12.5	9.5	/	/	31.1	35	23.2 (passive)	5.5 (passive)	27.1
3-dB Scanning Range (°)	±50°	±20°	/	/	±50°	<60°	N.A	N.A	±50°

*Note: Active components are not integrated in the fabricated array – only passive prototypes are demonstrated.

loss reaches around 5 dB when the beam scans to ±60° [see Fig. 20(a)]. At the band edges, the 3-dB beam scanning range is about ±48°. In the *x*-*z* plane, the 3-dB beam scanning range covers from −50° to 30° at 26.1 GHz, and from −48° to 30° at 25.7 and 27 GHz [see Fig. 20(b)]. The gain drop becomes more rapidly for beams pointing at positive angles due to the existence of the supporting acrylic structures and coaxial cable.

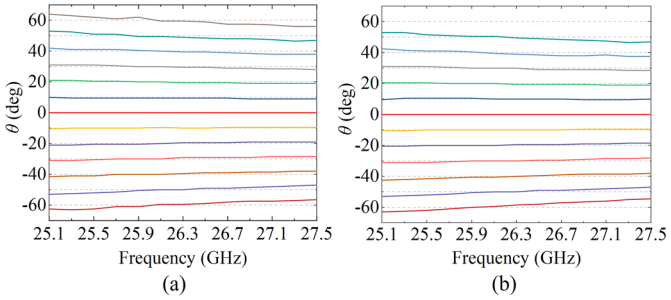

Fig. 21. Measured beam direction as a function of frequency in the (a) *y*-*z* plane and (b) *x*-*z* plane.

Furthermore, the beam direction as a function of frequency have also been measured in the range from 25.1 to 27.5 GHz. Within the ±60° scanning range, at 26.1 GHz, the maximum error of the beam pointing direction is less than 0.5°. As shown in Fig. 21, when the phase compensation is performed at a single frequency, the non-true-time-delay RRA experiences a small amount of beam pointing angle dispersion especially at large scanning angles. The variation of beam direction is about 1° for beams scanning within ±20° and about 3.5° for beams pointing at large angles of ±60° across the frequency band from 25.1 to 27.5 GHz.

Above all, the experimental results validate the proposed large-scale 2-bit RRA in the *Ka*-band, achieving the desirable beam scanning performance. A comparison between the proposed RRA and other previous reported works are shown in Table IV. It can be found that our design uses the fewest PIN diodes per polarization among the reported 2-bit unit cell. Compared to the mm-Wave 1-bit RRAs with aperture efficiencies of less than 13% due to the crude phase resolution [11], [26], the designed RRA achieves a much higher aperture efficiency of 27.1% benefiting from its 2-bit phase compensation. It can also be observed that most of the reported 2-bit RRAs designs are demonstrated only at the cell level or using frozen passive prototypes. This work realizes a fully-functional 2-bit mm-Wave RRA with a two-dimensionally steerable high-gain beam, which is superior in terms of the array scale, beam scanning performance, and system scalability.

V. CONCLUSION

In summary, the design, synthesis, implementation, and characterization of a large-scale 2-bit RRA operating at the *Ka*-band are presented. A miniaturized RRA cell offering the 2-bit reflection phase-shifting with a stable angular response is proposed, which is enabled by a segmented resonator with end folding and integrated with two PIN diodes. A free-space scattering measurement is performed to validate the proposed 2-bit RRA cells. For realizing large-scale RRAs, modular reflect-subarrays are employed as constitutive building blocks to construct extensible RRAs for versatile application purpose. As a proof-of-concept example, a 2-bit RRA prototype with 36 × 36 cells fed by a planar array is demonstrated. The measured results achieve beam scanning up to ±50° for a 3-dB scanning loss in two dimensions and an aperture efficiency of 27.1%, which is promising for various communication and radar applications. In addition, it is believed that the proposed 2-bit cell can be further extended for dual polarization, which is

currently being investigated.

ACKNOWLEDGMENT

The authors would like to express their gratitude to T. Y. Huo for his assistance during the antenna measurement.

REFERENCES

[1] J. Huang and J. A. Encinar, *Reflectarray Antennas*. New York, NY, USA: Wiley, 2008.

[2] P. Nayeri, F. Yang, and A. Z. Elsherbeni, *Reflectarray Antennas: Theory, Designs, and Applications*. Piscataway, NJ, USA: IEEE Press, 2018.

[3] S. V. Hum and J. Perruisseau-Carrier, "Reconfigurable reflectarrays and array lenses for dynamic antenna beam control: A review," *IEEE Trans. Antennas Propag.*, vol. 62, no. 1, pp. 183–198, Jan. 2014.

[4] P. Nayeri, F. Yang, and A. Z. Elsherbeni, "Beam scanning reflectarray antennas: A technical overview and state of the art," *IEEE Antennas Propag. Mag.*, vol. 57, no. 4, pp. 32–47, Aug. 2015.

[5] G. Perez-Palomino et al., "Accurate and efficient modeling to calculate the voltage dependence of liquid crystal-based reflectarray cells," *IEEE Trans. Antennas Propag.*, vol. 62, no. 5, pp. 2659–2668, May 2014.

[6] H. Kim, J. Kim, and J. Oh, "Liquid-crystal-based X-band reactively loaded reflectarray unit cell to reduce reflection loss," *IEEE Antennas Wireless Propag. Lett.*, vol. 20, no. 10, pp. 1898–1902, Oct. 2021.

[7] X. Yang et al., "A broadband high-efficiency reconfigurable reflectarray antenna using mechanically rotational elements," *IEEE Trans. Antennas Propag.*, vol. 65, no. 8, pp. 3959–3966, Aug. 2017.

[8] G.-B. Wu, S.-W. Qu, S. Yang, and C. H. Chan, "Low-cost 1-D beam-steering reflectarray with ±70° scan coverage," *IEEE Trans. Antennas Propag.*, vol. 68, no.6, pp.5009–5014, Jun. 2020.

[9] S. V. Hum, M. Okoniewski, and R. J. Davies, "Modeling and design of electronically tunable reflectarrays," *IEEE Trans. Antennas Propag.*, vol. 55, no. 8, pp. 2200–2210, Aug. 2007.

[10] M. E. Trampler, R. E. Lovato, and X. Gong, "Dual-resonance continuously beam-scanning X-band reflectarray antenna," *IEEE Trans. Antennas Propag.*, vol. 68, no. 8, pp. 6080–6087, Aug. 2020.

[11] H. Kamoda, T. Iwasaki, J. Tsumochi, T. Kuki, and O. Hashimoto, "60-GHz electronically reconfigurable large reflectarray using single bit phase shifters," *IEEE Trans. Antennas Propag.*, vol. 59, no. 7, pp. 2524–2531, Jul. 2011.

[12] H. Yang et al., "A 1-bit 10×10 reconfigurable reflectarray antenna: Design, optimization, and experiment," *IEEE Trans. Antennas Propag.*, vol. 64, no. 6, pp. 2246–2254, Jun. 2016.

[13] O. Bayraktar, O. A. Civi, and T. Akin, "Beam switching reflectarray monolithically integrated with RF MEMS switches," *IEEE Trans. Antennas Propag.*, vol. 60, no. 2, pp. 854–862, Feb. 2012.

[14] T. Debogovic and J. Perruisseau-Carrier, "Low loss MEMS reconfigurable 1-bit reflectarray cell with dual-linear polarization," *IEEE Trans. Antennas Propag.*, vol. 62, no. 10, pp. 5055–5060, Oct. 2014.

[15] J. Han, L. Li, G. Liu, Z. Wu, and Y. Shi, "A wideband 1 bit 12×12 reconfigurable beam-scanning reflectarray: design, fabrication, and measurement," *IEEE Antennas Wireless Propag. Lett.*, vol. 18, no. 6, pp. 1268–1272, Jun. 2019.

[16] B. J. Xiang, X. Dai, and K. -M. Luk, "A wideband low-cost reconfigurable reflectarray antenna with 1-bit resolution," *IEEE Trans. Antennas Propag.*, vol. 70, no.9, pp. 7439–7447, Sept. 2022.

[17] E. Carrasco, M. Barba, and J. A. Encinar, "X-band reflectarray antenna with switching-beam using PIN diodes and gathered elements," *IEEE Trans. Antennas Propag.*, vol. 60, no. 12, pp. 5700–5708, Dec. 2012.

[18] H. Yang, F. Yang, X. Cao, S. Xu, J. Gao, X. Chen, M. Li, and T. Li, "A 1600-element dual-frequency electronically reconfigurable reflectarray at X/Ku-band," *IEEE Trans. Antennas Propag.*, vol. 65, no. 6, pp. 3024–3032, Jun. 2017.

[19] X. Pan, F. Yang, S. Xu, and M. Li, "A 10240-element reconfigurable reflectarray with fast steerable monopulse patterns," *IEEE Trans. Antennas Propag.*, vol. 69, no. 1, pp. 173–181, Jan. 2021.

[20] F. Wu, R. Lu, J. Wang, Z. H. Jiang, W. Hong, and K.-M. Luk, "Circularly Polarized One-Bit Reconfigurable ME-Dipole Reflectarray at X-Band," *IEEE Antennas Wireless Propag. Lett.*, vol.21, no.3, pp. 496–500, Dec. 2022.

[21] Z. Wang et al., "1-bit electronically reconfigurable folded reflectarray antenna based on p-i-n diodes for wide-angle beam-scanning applications," *IEEE Trans. Antennas Propag.*, vol. 68, no. 9, pp. 6806–6810, Sept. 2020.

[22] H. Luyen, Z. Zhang, J. H. Booske, and N. Behdad, "Wideband, beamsteerable reflectarray antennas exploiting electronically reconfigurable polarization-rotating phase shifters," *IEEE Trans. Antennas Propag.*, vol. 70, no. 6, pp. 4414–4425, Jun. 2022.

[23] M.-T. Zhang et al., "Design of novel reconfigurable reflectarrays with single-bit phase resolution for Ku-band satellite antenna applications," *IEEE Trans. Antennas Propag.*, vol. 64, no. 5, pp. 1634–1641, May. 2016.

[24] J. Hu, P-L. Chi, and T. Yang, "Novel 1-bit beam-scanning reflectarray with switchable linear, left-handed, or right-handed circular polarization," *IEEE Trans. Antennas Propag.*, vol. 71, no. 2, pp. 1548–1556, Feb. 2023.

[25] H. Yu *et al.*, "Quad-polarization reconfigurable reflectarray with independent beam-scanning and polarization switching capabilities," *IEEE Trans. Antennas Propag.*, vol. 71, no. 9, pp. 7285–7298, July. 2023.

[26] X. Wan et al., "Reconfigurable sum and difference beams based on a binary programmable metasurface," *IEEE Antennas Wireless Propag. Lett.*, vol. 20, no. 3, pp. 381–385. Mar, 2021.

[27] H. Yang et al., "A study of phase quantization effects for reconfigurable reflectarray antennas," *IEEE Antennas Wireless Propag. Lett.*, vol. 16, pp. 302–305, Feb. 2017.

[28] C. Huang, B. Sun, W. Pan, J. Cui, X. Wu, and X. Luo, "Dynamical beam manipulation based on 2-bit digitally-controlled coding metasurface," *Sci. Rep.*, vol. 7, no. 1, p. 42302, Sept. 2017.

[29] J. Han et al., "Adaptively smart wireless power transfer using 2-bit programmable metasurface," *IEEE Trans. Ind. Electron.*, vol. 69, no. 8, pp. 8524–8534, Aug. 2022.

[30] L. L. Li et al., "Machine-learning reprogrammable metasurface imager," *Nature Commun.*, vol. 10, no. 1, p. 1082, Dec. 2019.

[31] X. Ma et al., "Design and Rectangular Waveguide Validation of 2-Bit Wideband Reconfigurable Reflective Metasurface Element in X-Band," *IEEE Antennas Wireless Propag. Lett.*, vol. 22, pp. 4–8, Jan. 2023.

[32] F. Wu *et al.*, "A 2 bit circularly polarized reconfigurable reflectarray using p-i-n-diode-tuned crossed-bowtie patch elements," IEEE Trans. Antennas Propag., vol. 71, no. 9, pp. 7299–7309, Sep. 2023.

[33] H. Luyen, J. H. Booske, and N. Behdad, "2-bit phase quantization using mixed polarization-rotation/non-polarization-rotation reflection modes for beam-steerable reflectarrays," IEEE Trans. Antennas Propag., vol. 68, no. 12, pp. 7937–7946, Jun. 2020.

[34] L. Dai et al., "Reconfigurable intelligent surface-based wireless communications: Antenna design, prototyping, and experimental results," *IEEE Access*, vol. 8, pp. 45913–45923, Mar. 2020.

[35] R. Pereira, R. Gillard, R. Sauleau, P. Potier, T. Dousset, and X. Delestre, "Dual linearly-polarized unit-cells with nearly 2-bit resolution for reflectarray applications in X-band," *IEEE Trans. Antennas Propag.*, vol. 60, no. 12, pp. 6042–6048, Dec. 2012.

[36] Q. Zhang *et al*., "A low-profile beam-steering reflectarray with integrated leaky-wave feed and 2-Bit phase resolution for Ka-band SatCom," *IEEE Trans. Antennas Propag.*, vol. 70, no. 3, pp. 1884–1894, Mar. 2022.

[37] C. C. Chieh and A. Abbaspour-Tamijani, "Evaluation of a novel topology for MEMS programmable reflectarray antennas," *IEEE Trans. Microw. Theory Techn.*, vol. 57, no. 12, pp. 3333–3344, Dec. 2009.

[38] L. Di Palma, A. Clemente, L. Dussopt, R. Sauleau, P. Potier, and P. Pouliguen, "1-bit reconfigurable unit cell for Ka-band transmitarrays," *IEEE Antennas Wireless Propag. Lett.*, vol. 15, pp. 560–563, 2016.

[39] N. Zhang et al., "A dual-polarized reconfigurable reflectarray antenna based on dual channel programmable metasurface," *IEEE Trans. Antennas Propag.*, vol. 70, no. 9, pp. 7403–7412 Sept. 2022.

[40] A. R. Vilenskiy, M. N. Makurin, C. Lee, and M. V. Ivashina, "Reconfigurable transmitarray with near-field coupling to gap waveguide array antenna for efficient 2-D beam steering," *IEEE Trans. Antennas Propag.*, vol. 68, no. 12, pp. 7854–7865, Dec. 2020.

[41] X. Tong, Z. H. Jiang, Y. Li, F. Wu, R. Sauleau, and W. Hong, "Dual-wideband dual-circularly-polarized shared-aperture reflectarrays with a single functional substrate for K-/Ka-band applications," *IEEE Trans. Antennas Propag.*, vol. 70, no. 7, pp. 5404–5417, Jul. 2022.

[42] A. E. Olk, and D. A. Powell, "Huygens metasurface lens for W-band switched beam antenna applications," *IEEE Open J. Antennas Propag.*, vol. 1, pp. 290–299, Jun. 2020.

[43] Z. H. Jiang, L. Kang, T. Yue, W. Hong, and D. H. Werner, "Wideband transmit arrays based on anisotropic impedance surfaces for circularly polarized single-feed multibeam generation in the Q-band," *IEEE Trans. Antennas Propag.*, vol. 68, no. 1, pp. 217–229, Jan. 2020

Enhao Wang was born in Huaian, Jiangsu, China, in 1995. He received the B.S. degree from Ocean University of China, Qingdao, China, in 2017, and the M.S. degree from Beijing University of Posts and Telecommunications, Beijing, China, in 2020. He is currently pursing the Ph.D degree with the School of Information Science and Technology in Southeast University, Nanjing, China. His main research interests include millimeter-wave antennas and reconfigurable reflectarray/transmitarray antenna designs.

Guangyao Peng was born in Nanjing, Jiangsu, China, in 1993. He received the B.S and M.S degrees from Southeast University, Nanjing, China, in 2016 and 2019, respectively. He is currently pursing the Ph.D degree with the School of Information Science and Technology in Southeast University, Nanjing, China. His main research interests include reconfigurable reflectarray and transmitarray.

Kunjing Zhong is currently an Engineer with the State Key Laboratory of Mobile Network and Mobile Multimedia Technology in ZTE Corporation, Shanghai, China.

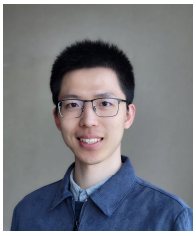

Fan Wu (S'15–M'18) was born in Jiangxi, China. He received the B.Eng and M.Eng degrees in electronic engineering from Beijing Jiaotong University, Beijing, China, in 2012 and 2015, respectively, and the Ph.D. degree in electronic engineering from City University of Hong Kong, Hong Kong, in 2018.

He is currently an Assistant Professor with the State Key Laboratory of Millimeter Waves, School of Information Science and Engineering, Southeast University, Nanjing, China. His current research is in the areas of space-fed antennas, circularly-polarized wideband antennas and reconfigurable antenna designs.

Dr. Wu was a recipient of the Honorable Mention at the student contest of the 2018 IEEE APS-URSI Conference and Exhibition held in Boston, USA. He served as a regular reviewer for numerous peer-reviewed international journals including the IEEE T-AP and AWPL.

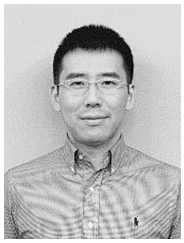

Zhi Hao Jiang (S'07–M'13) was born in Nanjing, China, in 1986. He received the B.S. degree in radio engineering from Southeast University, Nanjing, in 2008, and the Ph.D. degree in electrical engineering from The Pennsylvania State University, University Park, State College, PA, USA, in 2013. From 2013 to 2016, he was a Post-Doctoral Fellow with the Computational Electromagnetics and Antennas Research Laboratory, Department of Electrical Engineering, The Pennsylvania State University. He is currently a Professor with the State Key Laboratory of Millimeter Waves, School of Information Science and Engineering, Southeast University.

Dr. Jiang has authored or co-authored more than 120 papers in peer-reviewed journals, over 80 papers in conference proceedings, as well as 9 book chapters. He has also co-edited two books: *Electromagnetic Vortices: Wave Phenomena and Engineering Applications* (Wiley/IEEE Press, 2021), *Electromagnetics of Body-Area Networks: Antennas, Propagation, and RF Systems* (Wiley/IEEE Press, 2016). He holds 8 granted U.S. patents and 20 granted Chinese patents. He is serving as a committee member of the IEEE AP-S New Technology Direction Committee (NTDC) and IEEE MTT-S Diversity and Inclusion Committee (DIC) and has served as the TPC Co-Chair at multiple international conferences. He was a recipient of the ZTE Outstanding Collaboration Program Award in 2022, the Outstanding Youth Scholar of National Science Foundation of China in 2021, the IEEE Microwave Prize in 2021, the Young Scientist Award at the URSI-GASS in 2020, the Young Scientist Award at the 2019 ACES-China Conference, the High-Level Innovative and Entrepreneurial Talent presented by Jiangsu Province, China, in 2017, the Thousands of Young Talents presented by China government in 2016, the 2012 A. J. Ferraro Outstanding Doctoral Research Award in Electromagnetics, and several best (student) paper awards at international conferences. He is a Senior Member of CIE, serves as the Associate Editor of *IEEE Transactions on Antennas and Propagation*, *IET Communications*, was a Guest Editor of *International Journal of RF and Microwave Computer-Aided Engineering* and *Electronics Letters*. His current research interests include microwave/millimeter-wave antennas and circuits, millimeter-wave systems, impedance surfaces, metamaterials, and analytical methods.

Ronan Sauleau (M'04–SM'06–F'18) graduated in electrical engineering and radio communications from the Institut National des Sciences Appliquées, Rennes, France, in 1995. He received the Agrégation degree from the Ecole Normale Supérieure de Cachan, France, in 1996, and the Doctoral degree in signal processing and telecommunications and the "Habilitation à Diriger des Recherches" degree, both from the University of Rennes 1, France, in 1999 and 2005, respectively. He was an Assistant Professor and Associate Professor at the University of Rennes 1, between September 2000 and November 2005, and between December 2005 and October 2009, respectively. He has been appointed as a full Professor in the same University since November 2009. His current research fields are numerical modeling, millimeter-wave beam steering antennas, substrate integrated waveguide antennas, lens-based focusing devices, periodic and non-periodic structures (frequency selective surface (FSS), metasurfaces, polarizers, reflectarrays, and transmitarrays) and biological effects of millimeter waves.

He has been involved in more than 70 research projects at the national and European levels and has co-supervised 27 post-doctoral fellows, 57 PhD students and 50 master students.

He has received 20 patents and is the author or coauthor of more than 275 journal papers and 570 publications in international conferences and workshops. He was co-director of the research Department 'Antenna and Microwave Devices' at IETR and deputy director of IETR between 2012 and 2016. He is now director of IETR. Prof. Sauleau received the 2004 ISAP Conference Young Researcher Scientist Fellowship (Japan) and the first Young Researcher Prize in Brittany, France, in 2001 for his research work on gain-enhanced Fabry-Perot antennas. In September 2007, he was elevated to Junior member of the "Institut Universitaire de France". He was awarded the Bronze medal by Centre National de la Recherche Scientifique (CNRS) in 2008, and the silver medal in 2020. He received the 2021 Antenna EurAAP Award. He was the co-recipient of several international conference awards with some of his students (International School of Bioelectromagnetics 2005, Bioelectromagnetics Society (BEMS)'2006, Microwaves, Radar and Remote Sensing Symposium (MRRS)'2008, European Materials Research Society (E-MRS)'2011, BEMS'2011, International Microwave Symposium (IMS)'2012, Antenna Technology and Applied Electromagnetics (Antem)'2012, Bioelec-tromagnetics (BioEM)'2015, European Conference on Antennas and Propa-gation (EuCAP)'2019, and EuCAP'2021). He served as a guest editor for the IEEE Antennas Propogat. Special Issue on "Antennas and Propagation at mm and sub mm waves". He has served as a national delegate for several National Delegate for several European Cooperation in Science and Technology (EU COST) actions. He has served as a national delegate for European School of Antennas and Propagation (EurAAP) and as a member of the board of Director of EurAAP from 2013 to 2018.

Wei Hong (M'92–SM'07–F'12) received the B.S. degree from the University of Information Engineering, Zhengzhou, China, in 1982, and the M.S. and Ph.D. degrees from Southeast University, Nanjing, China, in 1985 and 1988, respectively, all in radio engineering.

He has been with the State Key Laboratory of Millimeter Waves, Southeast University, since 1988, where he has also been the Director of the Laboratory since 2003. He is currently a Professor of the School of Information Science and Engineering with Southeast University. In 1993 and 1995–1998, he was a short-term Visiting Scholar with the University of California at Berkeley and at Santa Cruz, CA, USA, respectively. He has authored or co-authored over 300 technical publications and authored two books. His current research interests include numerical methods for electromagnetic problems, millimeter-wave theory and technology, antennas, electromagnetic scattering, and RF technology for mobile communications

Dr. Hong was an Elected IEEE MTT-S AdCom Member during 2014–2016. He is a fellow of IEEE and Chinese Institute of Electronics (CIE). He twice awarded the National Natural Prizes, and thrice awarded the first-class Science and Technology Progress Prizes issued by the Ministry of Education of China and Jiangsu Province Government. Besides, he also received the Foundations for China Distinguished Young Investigators and for "Innovation Group" issued by the NSF of China. He is the Vice President of the CIE Microwave Society and Antenna Society and the Chair of the IEEE MTTS/APS/EMCS Joint Nanjing Chapter. He served as the Associate Editor of the IEEE TRANSACTIONS ON MICROWAVE THEORY AND TECHNIQUES from 2007 to 2010, and one of the Guest Editors for the 5G special issue of the IEEE TRANSACTIONS ON ANTENNAS AND PROPAGATION in 2017.